

A Unified Control Scheme for Track Seeking and Following of a Hard Disk Drive Servo System

Chin Kwan Thum, *Student Member, IEEE*, Chunling Du, *Senior Member, IEEE*, Ben M. Chen, *Fellow, IEEE*, Eng Hong Ong, and Kim Piew Tan

Abstract—This paper proposes a new nonlinear time-varying unified control scheme (UCS) for track-seeking and track-following in hard disk drives (HDDs) so as to avoid problem of mode switching. The proposed control scheme utilizes the concept of the conventional composite nonlinear feedback (CNF) scheme to achieve fast and smooth seeking. In order to be advantageous over the conventional CNF control, the UCS consists of both linear and nonlinear time-dependent components, which are independent of absolute seeking error. Simulation and implementation results show that, during track-seeking mode, the proposed scheme has a significantly better performance robustness against variations in seek length as compared to the conventional CNF control. For track-following, disturbance and noise models are involved in the problem formulation and sub-optimal H_∞ method is used to design the controller so as to achieve high head-positioning accuracy. It turns out that the unified controller removes 27.8% of the nonrepeatable disturbances and noise.

Index Terms—Hard disk drives (HDDs), mechatronics, mode switching, nonlinear time-varying systems (NLTV), servo systems.

I. INTRODUCTION

TO MEET THE continuing demand for faster data transfer rate and larger storage capacity in hard disk drives (HDDs), future HDD servo systems are required to have better seek-to-settle performance for shorter data execution time and less acoustic noise during track-seeking mode and higher precision head positioning accuracy during track-following mode (see Fig. 1 for a detailed illustration). To achieve such performances, minimum time control using nonlinear controllers such as proximate time optimal servomechanism (PTOS) [1] during track-seeking, and high precision control which is designed based on optimal linear control theories such as H_∞ [2], [3] and H_2 [3], [4] during track-following are naturally desired. As each of these control schemes for track-seeking and track-following has a totally different structure from the other, this leads to a mode switching control (MSC) system [3], [4], in which the specific servo controller is switched on as the HDD servo is performing in its corresponding mode of operation (see Fig. 2 for a detailed illustration). Special care must be taken to

Manuscript received June 23, 2008; revised December 24, 2008. Manuscript received in final form March 06, 2009. First published June 30, 2009; current version published February 24, 2010. Recommended by Associate Editor T. Zhang.

C. K. Thum and B. M. Chen are with the Department of Electrical and Computer Engineering, National University of Singapore, Singapore 117576. (e-mail: ckthum@nus.edu.sg).

C. K. Thum, C. Du, E. H. Ong, and K. P. Tan are with A*STAR Data Storage Institute, Singapore 117608.

Color versions of one or more of the figures in this paper are available online at <http://ieeexplore.ieee.org>.

Digital Object Identifier 10.1109/TCST.2009.2017513

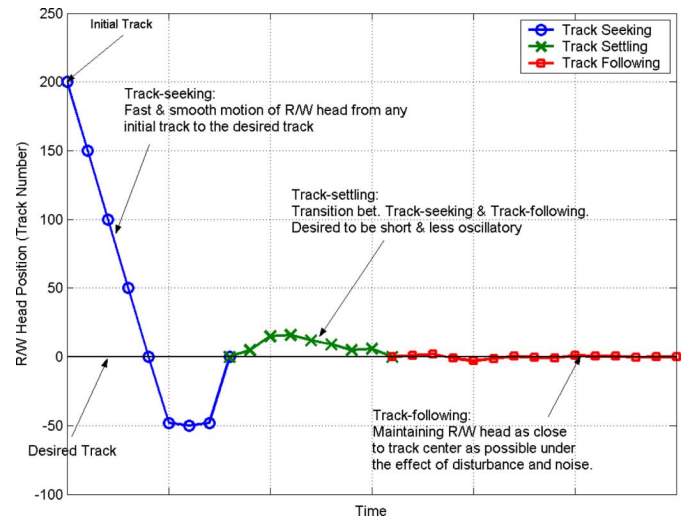


Fig. 1. Illustration of track-seeking, track-settling, and track-following of an HDD servo system.

avoid bad transient behaviors such as big overshoot and ringing upon every switching.

In order to avoid the MSC servo system so as to prevent its inherent transient problem upon switching, [5] proposes the discrete-time CNF control scheme, which is derived from its continuous counterpart [6], uses only a single nonlinear feedback controller to achieve fast track-seeking as well as high accuracy track-following performance. However, it is noted that though the design methodologies of the conventional CNF and its discretized counterpart [5], [6], [3] achieve excellent track seek-to-settle performance over PTOS and all other one-degree-of-freedom linear time-invariant feedback control schemes [4], [3], they suffer from bad performance robustness against slight variations in seek length and thus control designers have to spend many hours to design an effective high resolution gain scheduling [7] system that is supposed to work hand-in-hand with the nonlinear feedback controller to enhance the performance robustness of the overall servo system. Further, in order to avoid the excitation of undamped resonance modes during track-settling for short-span seeking [8] as well as to ensure performance robustness against plant variations, the final closed-loop system has a low servo bandwidth [3]. Thus naturally, the discrete-time CNF control scheme [5] is not a suitable choice for a unified control scheme for track-seeking and track-following of an HDD servo system [9]. Ever since then, several more modifications for the conventional CNF have been proposed. [10] extends CNF fast track performance to track non-setup references. [11] improves the performance

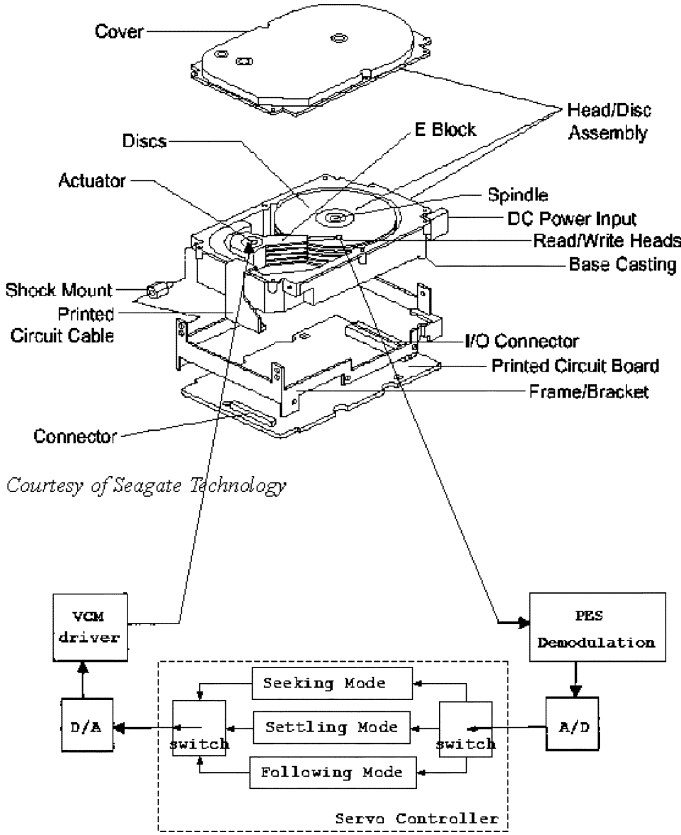


Fig. 2. Mechanical structure of a typical HDD and block diagram of its VCM-actuated servo system.

robustness against constant input disturbance of a CNF-controlled servo system. Though [12] manages to improve the conventional CNF performance by combining reference trajectory design which helps avoid controller saturation, it is not suitable for track-following due to the low servo bandwidth. Therefore, so far none of the modified CNF is a suitable choice to operate as a unified controller.

This paper proposes a nonlinear time-varying (NLTV) control scheme to further enhance the conventional CNF control so as to develop a significantly better unified control scheme for fast and smooth seeking and high precision track-following. The proposed unified control scheme contains a linear feedback law whose feedback gain is controlled by a nonlinear time-error function and a nonlinear time function, which ensures a fast response at the beginning of a track seek, a smooth settling response as time approaches the expected settling time t_s (error within $\pm 1\%$ of seek length), as well as a good disturbance and noise attenuation shortly after t_s . The advantages of the proposed control scheme can be listed as follows: 1) it is a unified controller for both track-seeking and track-following; 2) a linear and nonlinear time-dependent function associated with general parameters are employed so that it has more freedom to be designed and results in more robustness; and 3) disturbance and noise models are augmented with the plant so that a high accuracy track-following can be achieved. Its application in a 3.5-in HDD servo system will be demonstrated and simulation and implementation results will be shown to illustrate these advantages.

The outline of this paper is as follows. Section II briefly illustrates the servo system of a typical HDD as well as its modeling. Section III proposes the NLTV control scheme for both track-seeking and track-following. In Section IV, we will apply the proposed control scheme in an HDD servo system. Both simulation results and experimental results are presented to show how the proposed unified control scheme fares against the conventional CNF control in terms of track-seeking and track-following performance in Section V. Last, we draw some concluding remarks in Section VI.

II. SERVO SYSTEM OF AN HDD

Fig. 2 shows a typical HDD with a voice coil motor (VCM)-actuated servo system. It consists of a stack of flat rotating disks with positioning information or servo information embedded in their surfaces. The servo information is used to position the magnetic heads on the disk surfaces. Position measurement of the magnetic heads is achieved by means of analyzing the position error signal (PES) calculated from the read back signal.

The model of the plant to be controlled, i.e., the actuator mounted with the suspension, can be obtained by analytical derivation of actuator physics or system input-output identification. Analytical studies in [13] reveal that the plant model of a typical VCM actuator can be represented by a double integrator with some high frequency resonance modes and given by

$$P(s) = \frac{k_t k_v k_c}{m s^2} \prod \frac{s^2 + 2\zeta_{zi} w_{zi} s + w_{zi}^2}{s^2 + 2\zeta_{pi} w_{pi} s + w_{pi}^2} \quad (1)$$

where k_t is the current force constant, m is the mass of the actuator, k_y is position measurement gain, k_c is the current-voltage conversion gain, and w_{pi} and ζ_{pi} , respectively, stand for the center frequency and the damping ratio of the resonance modes of the actuator, whereas w_{zi} and ζ_{zi} , respectively, stand for the center frequency and the damping ratio of the anti-resonance modes of the actuator. Note that the VCM plant model depends on its geometry, mass, and material property, and thus analytical derivation to determine its accurate model requires much precise knowledge of the physical parameters of the actuator and suspension, while in laboratory studies, system identification based on frequency domain measurements in frequency domain is a more efficient and popular approach.

Hence, in this work, the actuator dynamics measurement is taken in the frequency domain. The VCM actuator is driven by a VCM driver which converts voltage differences into current differences linearly. The output of the plant, i.e., the displacement of the actuator, is measured by using a Polytec OFV 3001S Scanning Laser Doppler Vibrometer (LDV) in the range of $2 \mu\text{m}/\text{V}$. A dynamic signal analyzer (DSA) is used to generate a swept sine signal to excite the actuator and measure the actuator frequency response. The measured frequency response is shown in Fig. 3, where the modeled one is plotted from a 16th-order transfer function obtained using the curve-fitting method to approximate the measured frequency responses. The transfer function is given by

$$P(s) = \frac{2.18 \times 10^8}{s^2 + 1005s + 3.948 \times 10^5} P^d(s) \prod_{i=1}^6 P_i^{\text{rm}}(s) \quad (2)$$

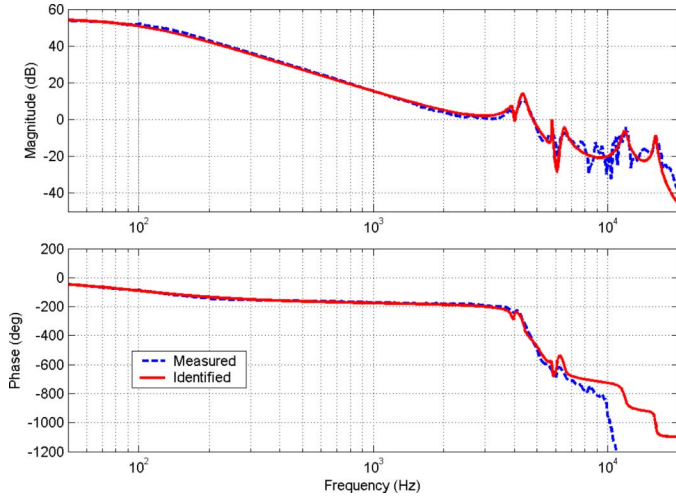


Fig. 3. Frequency responses of the VCM actuator (LDV range: $2 \mu\text{m/V}$).

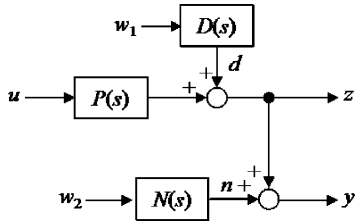


Fig. 4. Block diagram of a typical HDD servo system without any controller.

where the output is in micrometer and the input is in volts with $u_{\max} = 3 \text{ V}$. Its six main resonance modes are given by

$$P_1^{\text{rm}}(s) = \frac{0.9702s^2 + 487.7s + 6.13 \times 10^8}{s^2 + 990.2s + 6.13 \times 10^8} \quad (3)$$

$$P_2^{\text{rm}}(s) = \frac{0.563s^2 + 820s + 7.47 \times 10^8}{s^2 + 1367s + 7.47 \times 10^8} \quad (4)$$

$$P_3^{\text{rm}}(s) = \frac{0.91s^2 + 695.3s + 1.33 \times 10^9}{s^2 + 182.2s + 1.33 \times 10^9} \quad (5)$$

$$P_4^{\text{rm}}(s) = \frac{1.51s^2 - 7.95 \times 10^4s + 5.50 \times 10^9}{s^2 + 3411s + 5.50 \times 10^9} \quad (6)$$

$$P_5^{\text{rm}}(s) = \frac{1.17s^2 + 1.74 \times 10^5s + 1.01 \times 10^{10}}{s^2 + 2011s + 1.01 \times 10^{10}} \quad (7)$$

$$P_6^{\text{rm}}(s) = \frac{1.668 \times 10^9}{s^2 + 1634s + 1.668 \times 10^9}. \quad (8)$$

$P^d(s)$ is an all pass filter included to model any phase lag caused by system delay given by

$$P^d(s) = \frac{s^2 - 6535s + 1.07 \times 10^9}{s^2 + 6535s + 1.07 \times 10^9}. \quad (9)$$

Note that the low frequency mode in (2), which is different from the pure double integrator in (1), is due to the effect of pivot friction [14].

Fig. 4 is a block diagram that illustrates a simplified model of the HDD servo system without any controller. $P(s)$ represents the transfer function of the actuator plant. u is the control input. z is the true position error signal. y represents the measured position error signal. d represents the equivalent summed effect

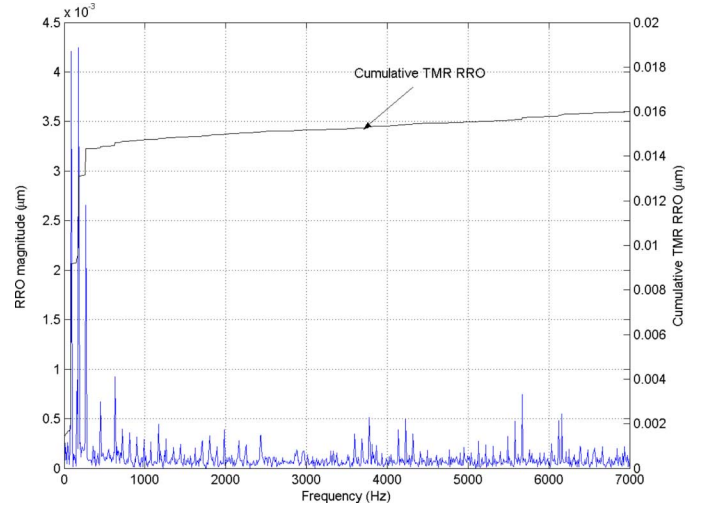


Fig. 5. Measured RRO power spectrum obtained from the STW platform in [15] prior to servo control.

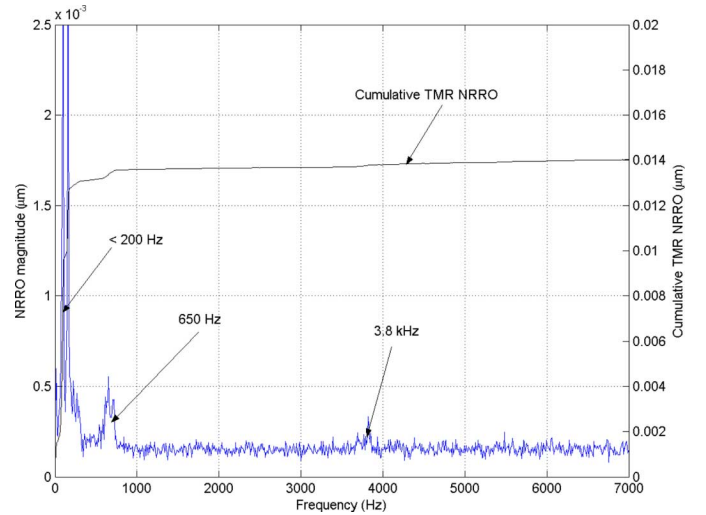


Fig. 6. Measured NRRO power spectrum prior to servo control.

of all disturbances. n denotes the PES measurement noise. w_1 and w_2 are the white noises with zero mean and unit variance. $D(s)$ and $N(s)$ are the disturbance and the noise models.

To have a high storage capacity in HDDs, the head positioning error with respect to the target track center needs to be as small as possible. The error are largely due to [3], [4]: 1) torque disturbances from spindle motor; 2) pivot friction of the actuator; 3) airflow-induced non-repeatable disk, actuator, and slider disturbances; 4) PES demodulation noise, media, quantization and electrical noise; and 5) eccentricity of tracks. The disturbances with their phase locked to the spindle rotation are classified as repeatable runout (RRO), and the others are classified as non-repeatable runout (NRRO).

In this paper, we adopt the disturbance and noise models of our servo track writer [15], which are similar to those in HDDs. Figs. 5 and 6 show the measured PES RRO and NRRO power spectra.

Using the method in [16], the true PES power spectrum and power density (PSD) can be approximated. Then the

calculated cumulative track misregistration (TMR) is given by [17]

$$\begin{aligned} \text{TMR} &= 3\sigma(\text{True PES}) \\ &= 3\sqrt{\frac{\sum_{i=1}^N \text{PSD}_i(\text{True PES})}{N}} \end{aligned}$$

where N represents the total number of true PES PSD data points. As such, corresponding to Figs. 5 and 6, the cumulative TMR RRO and NRRO are, respectively, calculated and shown in Figs. 5 and 6.

In Section III, we will propose a NLTV unified control scheme that is capable of achieving fast and smooth track-seeking as well as high accuracy track-following for the above mentioned HDD servo system.

III. UNIFIED CONTROL SCHEME FOR TRACK-SEEKING AND TRACK-FOLLOWING

The system, as seen in Fig. 4, can be described with a continuous-time linear time-invariant state-space representation Σ given by

$$\begin{aligned} \dot{x}(t) &= Ax(t) + B_1w(t) + B_2\text{sat}(u(t)), \quad x(0) = x_0 \\ y(t) &= C_1x(t) + D_{11}w(t) + D_{22}\text{sat}(u(t)) \\ z(t) &= C_2x(t) + D_{21}w(t) + D_{22}\text{sat}(u(t)) \end{aligned} \quad (10)$$

with

$$\begin{aligned} A &= \begin{bmatrix} A_p & 0 & 0 \\ 0 & A_d & 0 \\ 0 & 0 & A_n \end{bmatrix} \\ B_1 &= \begin{bmatrix} 0 & 0 \\ B_d & 0 \\ 0 & B_n \end{bmatrix} \\ B_2 &= \begin{bmatrix} B_p \\ 0 \\ 0 \end{bmatrix} \\ C_1 &= [C_p \quad C_d \quad C_n] \\ D_{11} &= [D_d \quad D_n] \\ C_2 &= [C_p \quad C_d \quad 0] \\ D_{21} &= [D_d \quad 0] \\ D_{22} &= D_p \end{aligned}$$

where $x(t)$, $u(t)$, $y(t)$, and $z(t)$ are, respectively, the combined states of $P(s)$, $D(s)$, and $N(s)$, the control input, the measurement output, and the controlled output. $w(t) = [w_1 \quad w_2]^T$. (A_p, B_p, C_p, D_p) , (A_d, B_d, C_d, D_d) , and (A_n, B_n, C_n, D_n) are, respectively, the matrix quadruple of $P(s)$, $D(s)$, and $N(s)$. Without loss of generality, $D_p = 0$. $\text{sat}: \mathfrak{R} \rightarrow \mathfrak{R}$ represents the actuator saturation defined as

$$\text{sat}(u(t)) = \text{sgn}(u(t)) \min\{u_{\max}, |u(t)|\}$$

with u_{\max} being the saturation level of the input. The following assumptions on the system matrices are required:

- 1) (A, B_2) is stabilizable;
- 2) (A, C_1) is detectable;
- 3) (A, B_2, C_2) is invertible and has no zeros at $s = 0$.

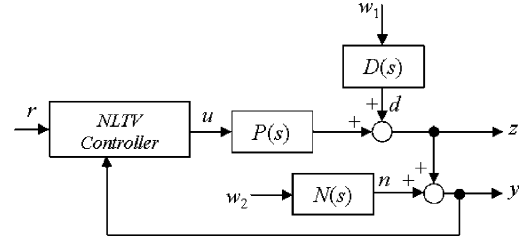


Fig. 7. Block diagram of the proposed NLTV control scheme.

A. Controller Structure

Here, we aim to design a nonlinear time-varying control law so as to achieve a fast and smooth track-seeking as well as high precision track-following performance. Motivated by [6], we have the following control law for the proposed unified control scheme:

$$u(t) = [F + \rho_2(t)F_f + \rho_1(t, y, r)F_s](x_v(t) - x_e) + Hr \quad (11)$$

where F , F_s , and F_f are gains to be designed, r is the reference input, $x_v(t)$ is the estimated states from the estimator given by

$$\dot{x}_v(t) = (A + KC_1)x_v(t) - Ky(t) + B_2\text{sat}(u(t)) \quad (12)$$

with the estimator gain K to be designed, H is given by

$$H := [1 - F(A + B_2F)^{-1}B_2]G \quad (13)$$

$$G = -[C_2(A + B_2F)^{-1}B_2]^{-1} \quad (14)$$

and

$$x_e := G_e r := -(A + B_2F)^{-1}B_2Gr. \quad (15)$$

$\rho_1(t, y, r)$ and $\rho_2(t)$ are scalar functions. For $\rho_1(t, y, r)$

- 1) $\rho_1(t, y, r) \in \mathfrak{R}$;
- 2) $0 \leq \rho_1(t, y, r) \leq 1 \quad \forall t$;
- 3) $\rho_1(t, y, r)$ saturates to unity before t_s ;
- 4) $\rho_1(t, y, r)$ is piecewise continuous in t ;
- 5) $\rho_1(t, y, r)$ is locally Lipschitz in y

and for $\rho_2(t)$

- 1) $\rho_2(t) \in \mathfrak{R}$;
- 2) $\rho_2(t) = 0 \quad \forall t < t_s$;
- 3) $\dot{\rho}_2(t) \geq 0 \quad \forall t$;
- 4) $\lim_{t \rightarrow \infty} \rho_2(t) = 1$;
- 5) $|\rho_2(t) - 1| \leq \frac{\kappa}{(t - \eta)^2} \forall t \geq t_1 > \eta$

for some positive scalars κ, η and a large t_1 .

The block diagram of the proposed control scheme is shown in Fig. 7.

Remark 1: Unlike the conventional CNF [6], the disturbance and noise model during track-following are augmented with the plant model so that we can include them in the design of the unified controller. Moreover, a nonlinear time-dependent function

$\rho_1(t, y, r)$ and a linear time-dependent function $\rho_2(t)$ instead of a single error-dependent nonlinear function are adopted to adjust the feedback gains. The advantages of this modification will become apparent in Section V, in which we will see how the modification helps improve seeking performance robustness against seek length variations as well as track-following performance. Additionally, instead of using $B_2^l P$, where P is the solution of a Lyapunov equation [6], to increase the damping of the closed-loop system of the plant dynamics, which dictates the seeking performance, towards the end of a seek for smooth settling, a general parameter F_s is used in (11) for the proposed scheme. This modification offers more degree of freedom in control design. The details on how F_s improves the damping of the closed-loop system of the plant dynamics will be discussed in Section III-C.

B. Stability Issues

We have the following theorem for the global exponential stability (GES) for the proposed control system.

Theorem 1: Consider the system (10) with the UCS control law (11) and the state estimator (12). Assume the disturbances and noise signals are zero, and the initial conditions x_0 , the required seek length r , the controller parameters K , F , F_s , F_f as well as $\rho_1(t, y, r)$ and $\rho_2(t)$ are properly selected or designed such that $|u(t)| \leq u_{\max}$, $\forall t \geq 0$, the proposed UCS control law (11) will drive the system output to track the reference track r asymptotically if both $A_p + B_p F_p$ and $A_p + B_p(F_p + F_{ps} + F_{pf})$ are asymptotically stable matrices and

$$\text{Re}[1 + G_1(j\omega)] > 0, \forall j\omega \geq 0 \quad (16)$$

where

$$G_1(j\omega) = -F_{ps}(j\omega I - A_p - B_p F_p)^{-1} B_p \quad (17)$$

with

$$(A_p + B_p F_p, B_p, -F_{ps}) \text{ minimal realization} \quad (18)$$

and F_p , F_{ps} , and F_{pf} are, respectively, composed of the first m columns of F , F_s , and F_f , and $m = \text{rank}(A_p)$.

The following lemma is used to prove *Theorem 1*. Its proof is given in *Lemma 2.2* in [20].

Lemma 1: Let A_x be an asymptotically stable matrix and $\int_{t_0}^{\infty} \|B_x(t)\| dt \leq b_x < \infty$ for some positive constant b_x . Then the origin of

$$\dot{x} = [A_x + B_x(t)]x, \quad \forall t \geq t_0. \quad (19)$$

is exponentially stable.

Proof: Let $\tilde{x} = x(t) - x_e$ and $\tilde{x}_v = x_v(t) - x(t)$. The estimator dynamics (12) and UCS control law (11) can be written as

$$\begin{aligned} \dot{\tilde{x}}_v &= (A + KC_1)\tilde{x}_v \\ u &= \{[F \quad F] + \rho_1(t, y, r)[F_s \quad F_s] \\ &\quad + \rho_2(t)[F_f \quad F_f]\} \begin{pmatrix} \tilde{x} \\ \tilde{x}_v \end{pmatrix} + Hr. \end{aligned} \quad (20)$$

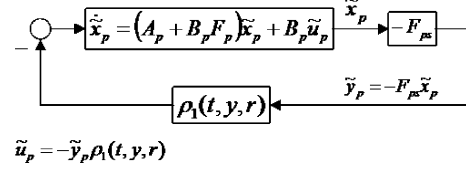


Fig. 8. Internal stability analysis diagram of \tilde{x}_p .

Considering $\rho_2(t) = 0$ at time $t < t_s$, the UCS control law (11) can be simplified as

$$u = \{[F \quad F] + \rho_1(t, y, r)[F_s \quad F_s]\} \begin{pmatrix} \tilde{x} \\ \tilde{x}_v \end{pmatrix} + Hr. \quad (21)$$

Here, for any r and x_0 the control parameters must be properly designed in a way such that $\forall t \geq 0$, $|u(t)| \leq u_{\max}$. This condition can be achieved by avoiding very large values of F , F_s , F_f in bid to achieve extreme performances. Consequently, the resulting closed-loop system with the UCS control law at time $t < t_s$ can be expressed as

$$\begin{pmatrix} \dot{\tilde{x}} \\ \dot{\tilde{x}}_v \end{pmatrix} = A_{\rho_1}(t, y, r) \begin{pmatrix} \tilde{x} \\ \tilde{x}_v \end{pmatrix} \quad (22)$$

where

$$\begin{aligned} A_{\rho_1}(t, y, r) &= \begin{bmatrix} A + B_2 F & B_2 F \\ 0 & A + KC_1 \end{bmatrix} \\ &\quad + \rho_1(t, y, r) \begin{bmatrix} B_2 F_s & B_2 F_s \\ 0 & 0 \end{bmatrix}. \end{aligned}$$

It is apparent that the system dynamics of \tilde{x}_v , which is given by $A + KC_1$, is time-invariant and asymptotically stable. Now, let $\tilde{x} = [\tilde{x}_p \quad \tilde{x}_d \quad \tilde{x}_n]'$, where \tilde{x}_p , \tilde{x}_d , and \tilde{x}_n are the elements of \tilde{x} that associated, respectively, with $P(s)$, $D(s)$, and $N(s)$. The system dynamics of \tilde{x}_d and \tilde{x}_n are obviously time-invariant and stable, though uncontrollable. Now we shall analyze the internal stability of \tilde{x}_p which can be illustrated using the block diagram as shown in Fig. 8.

Assuming $F_{ps}' F_{ps}$ is invertible, then

$$y = -C_p (F_{ps}' F_{ps})^{-1} F_{ps}' \tilde{y}_p + \xi(t) \quad (23)$$

where $\xi(t)$ is the lumped effect of x_e , \tilde{x}_d , and \tilde{x}_n . $\xi(t)$ may be unknown, but it is bounded and piecewise continuous in t . If we were to substitute (23) into $\rho_1(t, y, r)$, $\rho_1(t, y, r)$ in Fig. 8 may be replaced by a new nonlinear time-dependent function $\psi(t, \tilde{y}_p)$, which is a $[0, 1]$ -sector nonlinearity. Finally, given that $A_p + B_p F_p$ is Hurwitz and $1 + G_1(s)$ is strictly positive real, or equivalently, condition of (16) is satisfied, following the result of the Circle Criterion for absolute stability [7], \tilde{x}_p are global uniformly stable closed-loop states within the finite time period.

At time $t \geq t_s$, we have $\rho_1(t, y, r) = 1$. The UCS control law (11) is then given by

$$u = \{[F + F_s \quad F + F_s] + \rho_2(t)[F_f \quad F_f]\} \begin{pmatrix} \tilde{x} \\ \tilde{x}_v \end{pmatrix} + Hr. \quad (24)$$

Subsequently, the resulting closed-loop system with the UCS control law can be expressed as

$$\begin{pmatrix} \dot{\tilde{x}} \\ \dot{\tilde{x}}_v \end{pmatrix} = A_{\rho_2}(t) \begin{pmatrix} \tilde{x} \\ \tilde{x}_v \end{pmatrix} \quad (25)$$

where

$$A_{\rho_2}(t) = \begin{bmatrix} A + B_2(F + F_s) & B_2(F + F_s) \\ 0 & A + KC_1 \end{bmatrix} + \rho(t) \begin{bmatrix} B_2F_f & B_2F_f \\ 0 & 0 \end{bmatrix}.$$

Similarly, dynamics of \tilde{x}_r and \tilde{x}_n is stable while \tilde{x}_v is asymptotically stable. In this case, the internal dynamics of \tilde{x}_p is a linear time-varying and given by $A + B_2(F + F_s + \rho_2(t)F_{pf})$, which can be written as

$$\dot{\tilde{x}}_p = [A_p + B_p(F_p + F_{ps} + F_{pf}) + (\rho_2(t) - 1)F_{pf}] \tilde{x}_p. \quad (26)$$

Let

$$A_x = A_p + B_p(F_p + F_{ps} + F_{pf}) \quad (27)$$

$$B_x(t) = (\rho_2(t) - 1)F_{pf}. \quad (28)$$

Obviously, $\|B_x(t)\| < g$ for some constant since both $\rho_2(t)$ and F_{pf} are bounded functions. Considering $\|B_x(t)\| \leq \left\| \frac{\kappa}{(t-\eta)^2} F_{pf} \right\|, \forall t \geq t_1 > \eta$ for some positive scalars κ and η and a large t_1 , it becomes obvious that there exists a positive $b_x < \infty$ such that $\int_{t_0}^{\infty} \|B_x(t)\| dt \leq b_x$ with $t_0 = t_s$. Finally, according to Lemma 1, we can prove the global exponentially stability (GES) of \tilde{x}_p for $t \geq t_s$.

Ignoring the effect of disturbance and noise and combining the global uniformly stability result of \tilde{x}_p and \tilde{x}_v for $\forall t < t_s$ and the GES stability $\forall t \geq t_s$, we have the complete proof of the GES stability of the resulting closed-loop system for $\forall t \geq 0$. Thus, $\lim_{t \rightarrow \infty} \tilde{x}(t) = 0$. Consequently

$$\lim_{t \rightarrow \infty} x(t) = x_e \quad (29)$$

and hence

$$\lim_{t \rightarrow \infty} z(t) = \lim_{t \rightarrow \infty} C_2 x(t) = C_2 x_e = r. \quad (30)$$

This completes the proof of *Theorem 1*.

C. Design of Controller Parameters

1) *Design of K and F*: K may be designed using any methods as long as $A + KC_1$ is asymptotically stable.

While $t < t_s$, the expected settling time, the dominant poles of the closed-loop system of the plant dynamics are given by the dominant B_2 -affine eigenvalues of $A + B_2(F + \rho_1(t, y, r)F_s)$. Thus, F can be designed using the pole-placement method such that the dominant B_2 -affine closed-loop plant poles for $\rho_1(t, y, r) = 0$ provide a rise time faster than t_s . This is to ensure a fast response at the beginning of a track seek so that it is possible to achieve an error within $\pm 1\%$ of seek length r by time t_s . If there is no value of F to achieve a rise time faster than t_s with $|u(t)| \leq u_{\max}$, the specified t_s is too short and has to be increased.

2) *Design of F_s and $\rho_1(t, y, r)$* : $\rho_1(t, y, r)$ performs the function to increase the damping of the closed-loop system of the plant dynamics drastically as the error is getting smaller so as to minimize the overshoot. It is designed in a way such that it remains near to zero when the tracking error is large and approaches unity when tracking error is small. Thus, F_s can be designed using the pole-placement method such that the dominant poles of the closed-loop system of the plant dynamics when $\rho_1(t, y, r) = 1$ have a large damping ratio. Finally, as time approaches t_s , i.e., when the seeking error is expected to be very small, $\rho_1(t, y, r)$ is independent of y and r and saturates to unity before time t_s .

In this paper, our choice for $\rho_1(t, y, r)$ takes the form

$$\rho_1(t, y, r) = \frac{[e^{-\alpha|y/r|-1} - e^{-\alpha}]}{1 - e^{-\alpha}}, \quad t < \beta t_s \quad (31)$$

$$\rho_1(t, y, r) = 1, \quad \text{else} \quad (32)$$

where α is a positive scalar designed in a way such that $\rho_1(t, y, r)$ increases from zero to unity as seeking error reduces. And at time βt_s ($0 < \beta < 1$), $\rho_1(t, y, r)$ saturates to unity. Note that as seeking error is expected to be very small prior to βt_s , given that β is sufficiently close to unity, the transition of $\rho_1(t, y, r)$ between time βt_s^- and βt_s^+ will be generally smooth.

Remark 2: The conventional CNF control [6] uses the nonlinear function $\rho(e)$ depends on the absolute value of e , and the set of parameters for $\rho(e)$ needs to be redesigned accordingly as the reference input r varies slightly. In the proposed control law, $\rho_1(t, y, r)$ is dependent on the ratio between error and $|r|$. This modification greatly reduces the seeking performance sensitivity against seek length variations. Hence, a carefully chosen $\rho_1(t, y, r)$ will achieve excellent track-seeking performance within a relatively wider range of r .

3) *Design of F_f and $\rho_2(t)$* : Note that after the time approaches t_s , $\rho_2(t)$ rises from zero and approaches unity gradually. This implies the servo system should be gradually switching its operation mode from seeking to track-following. Thus, designers should design F_f in a way such that, the effect of disturbance and measurement noise is effectively attenuated to achieve high precision positioning performance. Any controller design methods based on the state-space approaches, such as LQG/LTR [18] or the robust and the perfect tracking design technique [3] are applicable. Note that when $\rho_2(t) = 1$, the transfer function from $w(t)$ to $z(t)$ is given by

$$T_{zw}(s) \approx C_2(sI - A - B_2(F + F_s + F_f))^{-1} B_1. \quad (33)$$

Control designers may either try to reduce $\|T_{zw}\|_{\infty}$ using H_{∞} design methods [2] or try to minimize $\|T_{zw}\|_2$ using H_2 control [3] design methods to design F_f so as to achieve high track-following precision.

In this paper, our choice of $\rho_2(t)$ is given by

$$\rho_2(t) = 0, \quad , \quad t < t_s + \epsilon \quad (34)$$

$$\rho_2(t) = 1 - \exp\left[-\gamma(t - t_s - \epsilon)^2\right], \quad \text{else} \quad (35)$$

where ϵ and γ are positive scalars that determine how fast $\rho_2(t)$ approaches unity, which in turn decides how fast the set of con-

trol parameters of the UCS controller is tuned from the one that is optimized for rapid track-seeking to another which is optimized for high accuracy track-following. Though a large γ ensures a fast switch between different modes of operation, it is noted if $\rho_2(t)$ varies too fast, a rapid change in control signal may cause undesirable excitations of poorly damped actuator modes to occur.

IV. CONTROLLER DESIGN FOR AN HDD SERVO SYSTEM

In this section, we proceed to design a servo control system for the HDD with the models in Section II.

After being precompensated by three second-order notch filters given by

$$F_1^{nf}(s) = \frac{s^2 + 1913s + 7.47 \times 10^8}{s^2 + 2.624 \times 10^4s + 7.47 \times 10^8} \quad (36)$$

$$F_2^{nf}(s) = \frac{s^2 + 3770s + 5.69 \times 10^9}{s^2 + 3.77 \times 10^4s + 5.69 \times 10^9} \quad (37)$$

$$F_3^{nf}(s) = \frac{s^2 + 5027s + 1.011 \times 10^{10}}{s^2 + 5.03 \times 10^4s + 1.011 \times 10^{10}} \quad (38)$$

the plant model $P(s)$ in (2) can be approximated by the second-order model

$$P_{comp}(s) = F_1^{nf}(s)F_2^{nf}(s)F_3^{nf}(s)P(s) \approx \frac{2.18 \times 10^8}{s^2 + 1005s + 3.948 \times 10^5}. \quad (39)$$

In order to achieve a satisfying sensitivity and complementary gain function, i.e., respectively, $|T_{zd}|$ and $|T_{zn}|$, during track-following mode for good disturbance and noise attenuation, H_∞ loop shaping method shall be used. Consequently, $D(s)$ and $N(s)$ in Figs. 4 and 7 can be used as weighting functions for the H_∞ problem formulation. With the measured RRO and NRRO power spectrum as shown in Figs. 5 and 6 in mind. $D(s)$ and $N(s)$ are designed to be given by

$$D(s) = \frac{0.0005968s^3 + 18s^2 + 7.91 \times 10^4s + 9.475 \times 10^7}{s^3 + 263.9s^2 + 2.175 \times 10^4s + 5.73 \times 10^5} \quad (40)$$

and

$$N(s) = 0.004376. \quad (41)$$

Since the designed controller order is equal to the order of the augmented plant in (10), to have a lower order controller it is wise to use the precompensated plant (39), which has a lower order than the full plant model (2). With the given $P_{comp}(s)$ in (39), $D(s)$ in (40) and $N(s)$ in (41), it is easy to verify that all the three assumptions for the proposed UCS control scheme are fully satisfied. Next, we will design a UCS control scheme for 0.2, 2, and 20 μm seek lengths with zero initial conditions for $t_s = 1$ ms.

Using the pole-placement method, F is obtained as

$$F = [-0.0973 \quad 3.4587 \times 10^{-7} \quad 0 \quad 0 \quad 0] \quad (42)$$

which places the dominant poles of the closed-loop system of the plant dynamics for $\rho_1(t) = 0$ at $-464.8 \pm j4624.9$. We note that the rise time of the closed-loop system for $\rho_1(t, y, r) = 0$ is much faster than the chosen t_s .

Next, F_s is designed using pole-placement method again to place the two most dominant poles of the closed-loop system of the plant dynamics for $\rho_1(t, y, r) = 1$ at -2168 and $-14\text{thinspace}836$ to increase the damping of T_{zr} drastically to reduce overshoot as ρ_1 approaches unity or as time approaches βt_s . It is given by

$$F_s = [-0.048398 \quad -7.3733 \times 10^{-5} \quad 0 \quad 0 \quad 0]. \quad (43)$$

F_f is obtained using the H_∞ -ARE method [3], [4] that aims to minimize $\|T_{zw}\|_\infty$ for high precision track-following performance. It is given by

$$F_f = [-51780 \quad -1.0001 \quad -29859 \quad -2.547 \times 10^5 \quad -1.1697 \times 10^6]. \quad (44)$$

The estimator gain K is designed using LTR method [3] to recover the performance achieved by the state feedback control law. It is given by

$$K = [-770.65 \quad 3404.2 \quad -6217.3 \quad -604.78 \quad -15.653]'. \quad (45)$$

In function $\rho_1(t, y, r)$ of (31)–(32), $\alpha = 0.45$ and $\beta = 0.9$, and in function $\rho_2(t)$ of (34)–(35), $\gamma = 30000$ and $\epsilon = 0.5$ ms.

Note that both $\rho_1(t, y, r)$ and $\rho_2(t)$ satisfy all the conditions listed in *Theorem 1*. And it is easy to verify that with the designed $\rho_2(t)$, when $t \geq 6.87$ ms, $\rho_2(t) > 0.9 \approx 1$. This implies that by 6.87 ms since the start of a seek command, the UCS control parameters have been adjusted nearly completely for sub-optimal H_∞ track-following performance.

In what follows, we analyze the GES stability of the designed control system. It is easy to verify that both $A_p + B_p F_p$ and $A_p + B_p (F_p + F_{ps} + F_{pf})$ are Hurwitz and $F'_{ps} F_{ps}$ is invertible. Following the result of *Theorem 1*, (16) is important to the GES stability of the resulting closed-loop system. From the designed controller parameters, $G_1(s)$ is given by

$$G_1(s) = \frac{1.607 \times 10^4 s + 1.055 \times 10^7}{s^2 + 929.6s + 2.161 \times 10^7}.$$

Its Nyquist plots is shown in Fig. 9, where it is apparent that condition of (16) is satisfied. Thus, following the result of *Theorem 1*, the resulting closed-loop system is GES stable.

For comparison, we also design a conventional CNF controller, which is solely optimized for 2 μm seeking with zero initial conditions, by using the MATLAB toolkit [19]. It is given by

$$\dot{x}_v(t) = \begin{bmatrix} -2032.7 & 1 \\ -2.571 \times 10^6 & -1005 \end{bmatrix} x_v(t) + \begin{bmatrix} 2032.7 \\ 2.1762 \times 10^6 \end{bmatrix} y(t) + \begin{bmatrix} 0 \\ 2.18 \times 10^8 \end{bmatrix} \text{sat}(u(t)) \quad (46)$$

and

$$u(t) = \{[-0.0996 \quad 2.9742 \times 10^{-7}] + \rho(e) [0.0493 \quad 7.5654 \times 10^{-5}]\} \left(x_v(t) - \begin{bmatrix} r \\ 0 \end{bmatrix} \right) + 0.1014r \quad (47)$$

where

$$\rho(e) = -2.80 [\exp(-0.65|e|) - 0.5220]. \quad (48)$$

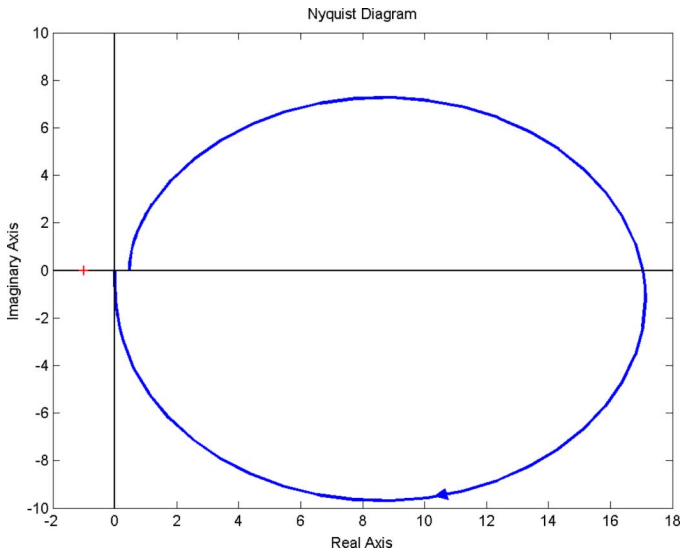
Fig. 9. Nyquist plot of $G_1(s)$.

TABLE I
COMPARISON OF OPERATION NUMBERS OF THE TWO CONTROL SCHEMES

Operation	CNF	UCS
$\exp(\cdot)$	1	2
$\int(\cdot)$	2	5
\times	15	34
$+$	12	32

Compared with the conventional CNF design, the proposed UCS control law (11) requires a higher dynamical order and demands a higher computation power for state estimation and the calculation of the instantaneous feedback gains. Table I shows the approximate computation cost of the two controllers.

V. SIMULATION AND IMPLEMENTATION RESULTS

This section will present the simulation and implementation results to verify the effectiveness of the proposed control scheme. We will compare the performance robustness of the proposed UCS to that of the conventional CNF scheme through simulation. All the simulation results are obtained using the MATLAB package, SIMULINK. In the experiment, we will demonstrate the 0.2, 2, and 20 μm track-seeking performance achieved by the proposed UCS as well as the 2 μm tracking-seeking performance achieved by the conventional CNF scheme. The experimental setup is shown in Fig. 10, where a dissected HDD is placed on a vibration free platform, the displacement of the R/W head is measured via a scanning LDV, and the control law is discretized using bilinear rule at a sampling frequency of 40 kHz and implemented via a dSpace DSP installed on a desktop PC. The VCM driver input voltage is kept within $[-3\text{ V}, 3\text{ V}]$.

A. Simulation Results

In what follows, we will show the simulation results with comparison to the conventional CNF scheme in terms of the performance robustness against variations in seek length and plant uncertainty.

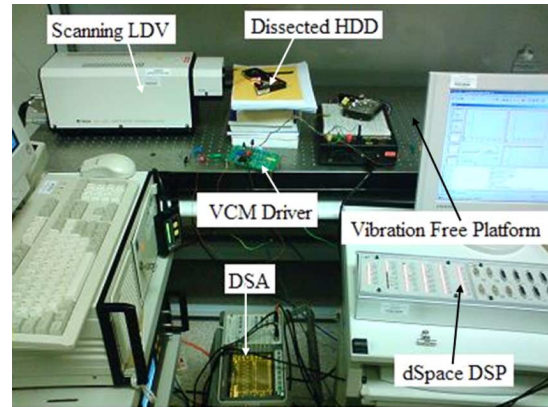
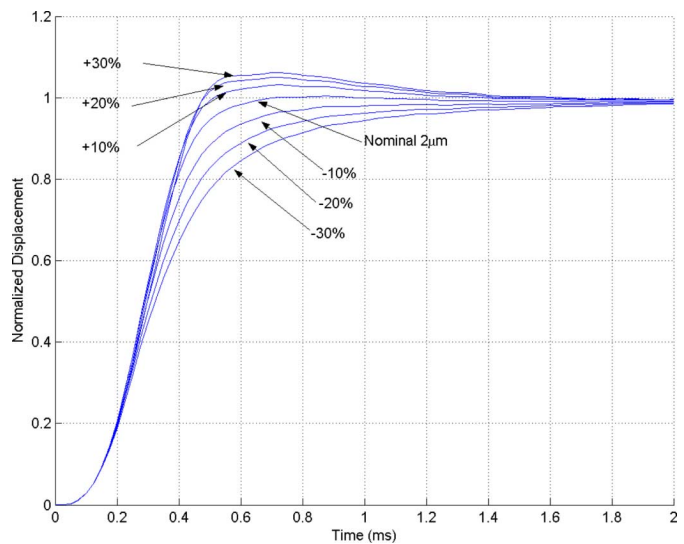


Fig. 10. Experimental setup.

Fig. 11. Simulation results: Normalized responses under a single conventional CNF control law whose design parameters are optimized for the nominal 2 μm seek.

1) *Seeking Performance Robustness Against Small Variation in Seek Length:* The seeking performances with small seek length variations from the nominal 2 μm are shown in Fig. 11 with the conventional CNF design and 12 with the proposed UCS design. It is seen that the proposed UCS is much less sensitive than the conventional CNF control scheme to any changes in seek length. This is because in the proposed scheme, the nonlinear time-varying function $\rho_1(t, y, r)$ is dependent on error-over-seeklength ratio instead of the absolute error. Thus, it is independent of the target seek length. Consequently, the overall closed-loop system is seek-length independent, whereas the conventional CNF control scheme is seek-length dependent and optimized specifically for 2 μm seek, and thus it cannot achieve the same performance properly for other seek lengths.

2) *Seeking Performance Robustness Against Plant Uncertainty:* During seeking process, i.e., $t \leq t_s$, the servo control system is designed to have the low servo bandwidth between 400 to 700 Hz. Hence, their seeking performances are typically immune to plant uncertainty. In terms of $\pm 10\%$ variations in the damping and frequency of plant resonances, Fig. 13 shows the simulation results obtained when using the proposed scheme. It

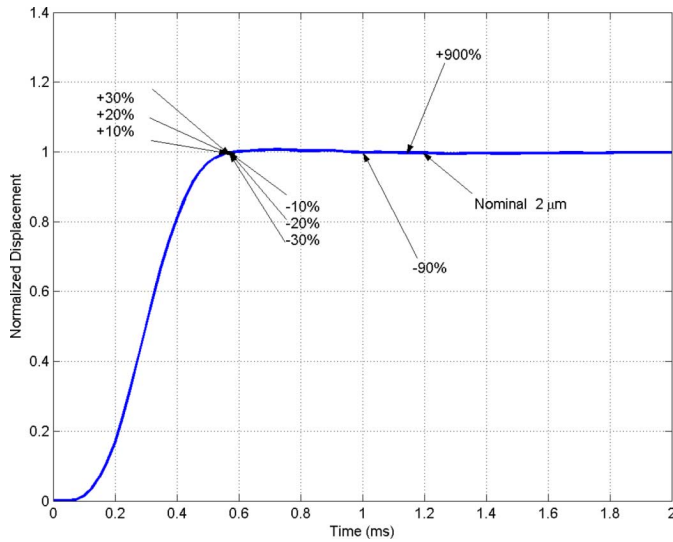


Fig. 12. Simulation results: Normalized responses under a single UCS control law whose design parameters are optimized for the nominal $2 \mu\text{m}$ seek.

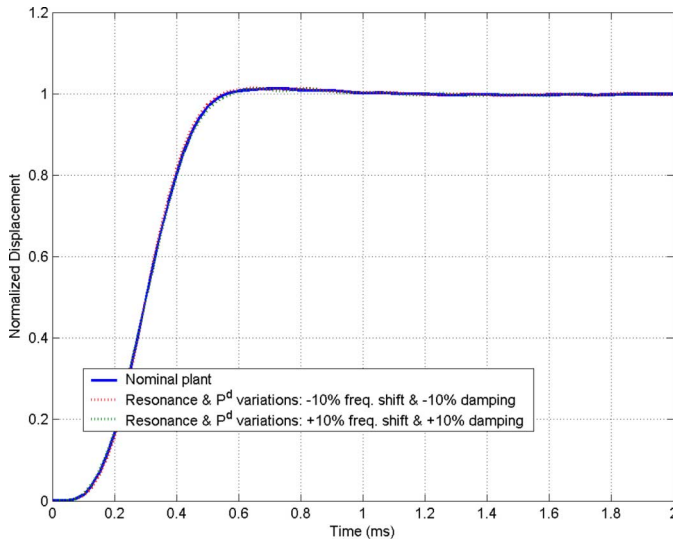


Fig. 13. Simulation results: Nominal seeking performance robustness of the proposed scheme against plant uncertainty.

is noted that the conventional CNF control scheme has similar robustness.

B. Implementation Results

1) *Seeking Performance*: Figs. 14 and 15 show the $2 \mu\text{m}$ seeking performance of respective control schemes. From the figures, it is clear that our proposed scheme can achieve a comparable fast seeking performance with a settling time (error within $\pm 1\%$ of seek length) of 0.6 ms to that of the conventional CNF control scheme whose design parameters are optimized for this particular seek length and have achieved a settling time of 0.65 ms . Figs. 15–17 shows that the proposed scheme has met the design specifications and also achieved a short settling time of 0.6 ms for $0.2, 2,$ and $20 \mu\text{m}$ seeking.

Moreover, to provide the experimental proofs for our claims about the improved performance robustness against variations

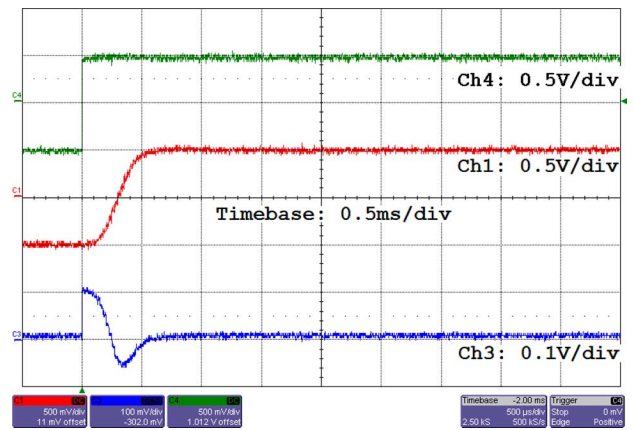


Fig. 14. CNF: $2 \mu\text{m}$ seek, Ch1: LDV-measurement ($2 \mu\text{m/V}$), r , Ch3: VCM-driver input, $u, y(t)$, Ch4: Seek Command Input ($2 \mu\text{m/V}$).

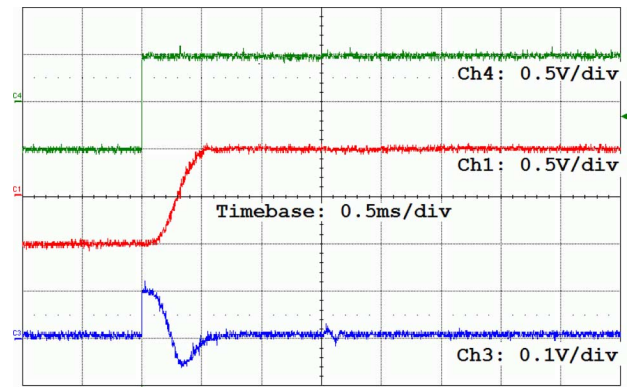


Fig. 15. UCS: $2 \mu\text{m}$ seek, Ch1: LDV-measurement ($2 \mu\text{m/V}$), r , Ch3: VCM-driver input, $u, y(t)$, Ch4: Seek Command Input ($2 \mu\text{m/V}$).

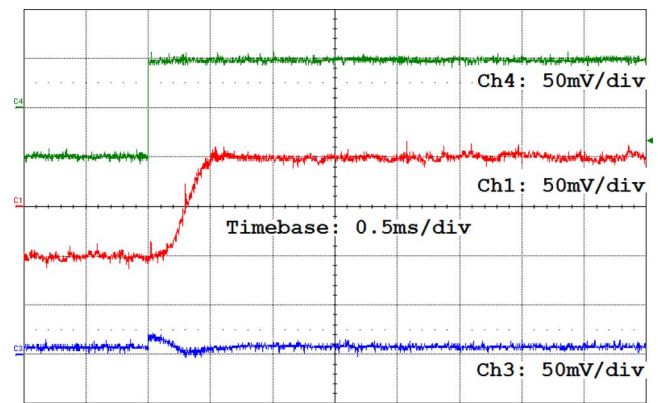


Fig. 16. UCS: $0.2 \mu\text{m}$ seek, Ch1: LDV-measurement ($2 \mu\text{m/V}$), r , Ch3: VCM-driver input, $u, y(t)$, Ch4: Seek Command Input ($2 \mu\text{m/V}$).

in seek-length achieved with the proposed scheme, more step response experiments are carried out. Fig. 18 shows how the conventional CNF seeking performance achieved by the nominal controller deteriorate as we vary the seek-length slightly. We have summarized the experimental outcomes in Table II.

Remark 4: Note that during our experiment, when γ in $p_2(t)$ (35) is larger than 10^4 , we begin to observe ringing effect at the measured output y when controller feedback gains switching from track-seeking and track-following. This is likely caused by

TABLE II
COMPARISON OF SETTLING TIME (MILLISECONDS) WITH DIFFERENT CONTROL SCHEMES AGAINST VARIATIONS IN SEEK LENGTH (NOMINAL SEEK LENGTH: 2 μm)

Scheme	Seek length variations				
	0% (Nominal)	-20 %	+20 %	-90 % (0.2 μm)	+900 % (20 μm)
CNF	0.65	1.5	1.5	—	—
UCS	0.6	0.6	0.6	0.6	0.6

“—” : untested

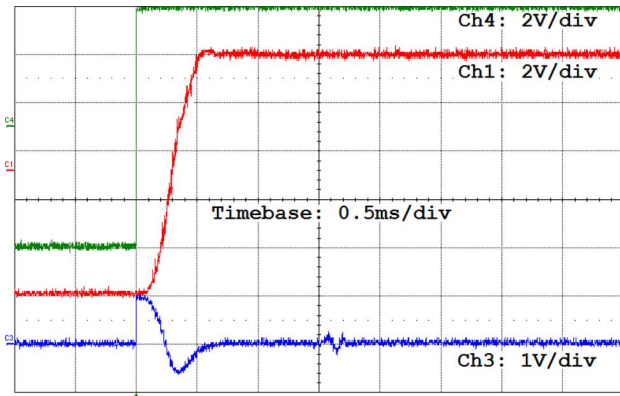


Fig. 17. UCS: 20 μm seek, Ch1: LDV-measurement (2 $\mu\text{m}/\text{V}$), r , Ch3: VCM-driver input, u , $y(t)$, Ch4: Seek Command Input (2 $\mu\text{m}/\text{V}$).

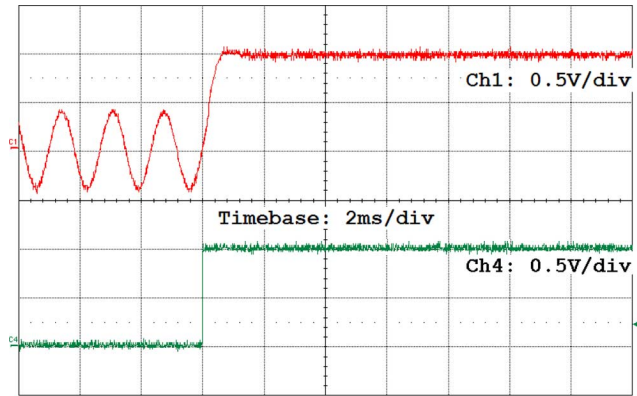


Fig. 19. UCS performance robustness against initial velocity of 3 mm/s. Ch1: LDV-measurement (2 $\mu\text{m}/\text{V}$), Ch4: Trigger. Indicates the start of a nominal 2 μm seek.

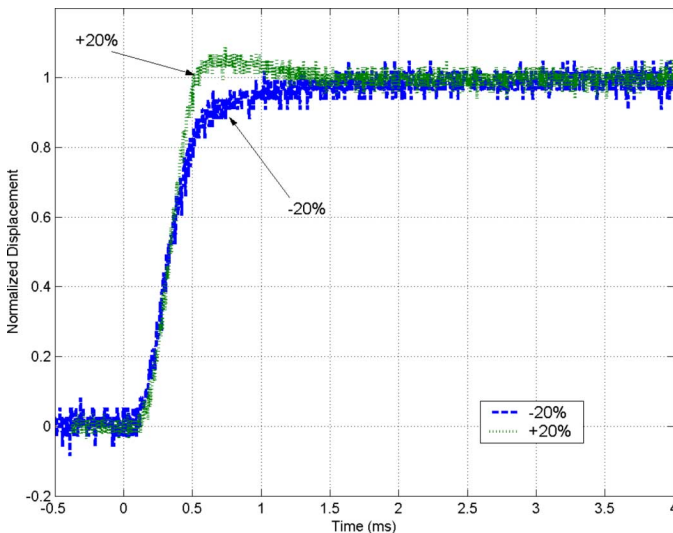


Fig. 18. Experimental results: Conventional CNF performance robustness against $\pm 20\%$ variation in the nominal seek length.

undesirable excitation of poorly damped actuator modes that occurs due to a rapid change in control signal u .

2) *Seeking Performance Robustness Against Variations in Initial Condition:* Here, we seek to examine the seeking performance robustness against variation in velocity. In our experiment, the R/W head is made to track a 600 Hz sinusoidal waveform initially with a linear time-invariant controller prior to switching to the proposed control scheme for a nominal 2 μm seek. Figs. 19–21 show the experimental results. For a nominal 2 μm seek, owing to the capability of the closed-loop system to adjust its damping ratio appropriately during a seek, from Figs. 19 and 20, it is apparent that the initial velocity of 6 mm/s or lower hardly affects the seeking performance in terms of overshoot and settling time. However, it is noted that as the initial

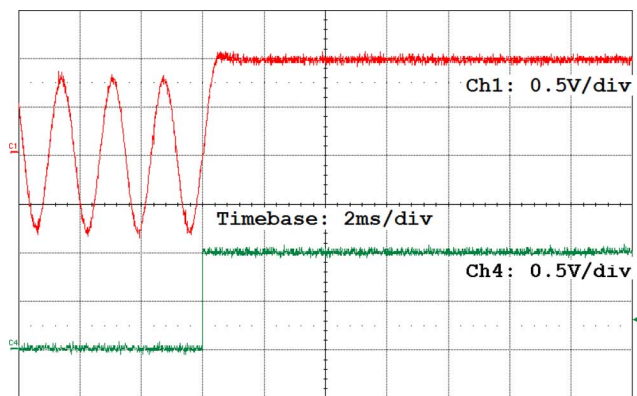


Fig. 20. UCS performance robustness against initial velocity of 6 mm/s. Ch1: LDV-measurement (2 $\mu\text{m}/\text{V}$), Ch4: Trigger. Indicates the start of a nominal 2 μm seek.

velocity increases beyond 6 mm/s, the overshoot gets larger and the settling time becomes longer. As shown in Fig. 21, when the initial velocity is increased to 12 mm/s, the size of overshoot is about 15% and the settling time is increased to approximately 1 ms. Fig. 22 analyzes the effect of non-zero initial acceleration. From the figure, it is known that the seeking performance is less sensitive to variation in initial acceleration as compared to variation in initial velocity. The details are summarized in Table III. Additionally, it should be mentioned that the conventional CNF control scheme displays similar robustness.

3) *Seeking Performance With the Effect of Disturbance and Noise:* Under the effect of disturbances and measurement noise, the nominal 2 μm seeking with the respective control scheme is shown in Fig. 24. In this case, RRO and NRRO having same amplitude and with the spectrum in Figs. 5 and 6 are injected into the closed-loop system. To avoid the effect of non-initial conditions, the disturbances are injected only from the start of

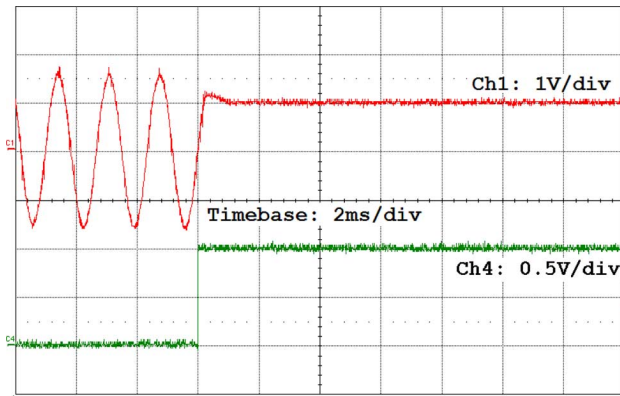


Fig. 21. UCS performance robustness against initial velocity of 12 mm/s. Ch1: LDV-measurement ($2 \mu\text{m/V}$), Ch4: Trigger. Indicates the start of a nominal $2 \mu\text{m}$ seek.

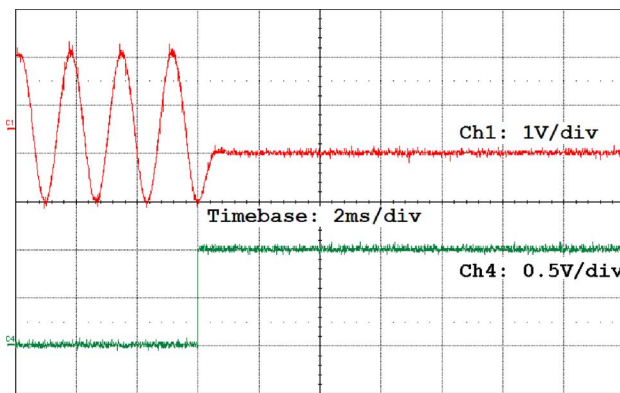


Fig. 22. UCS performance robustness against initial acceleration of $4.5 \times 10^3 \text{ mm/s}^2$. Ch1: LDV-measurement ($2 \mu\text{m/V}$), Ch4: Trigger. Indicates the start of a nominal $2 \mu\text{m}$ seek.

TABLE III
NOMINAL $2 \mu\text{m}$ SEEKING PERFORMANCE SUMMARY WITH THE PROPOSED SCHEME AGAINST VARIATIONS IN INITIAL CONDITION

Initial cond.		Settling time (ms)	Overshoot (%)
Velocity (mm/s)	3	0.6	2
	6	0.65	5
	12	1	15
Acceleration (10^3 mm/s^2)	4.5	0.65	2

the seeks. The 3% settling time with the proposed scheme is found to be approximately 1.0 ms. During the track-following mode, the proposed scheme has achieved a significantly higher head positioning accuracy as seen in Fig. 24. With the conventional CNF, the output never settles down within the range of $2 \pm 3\% \mu\text{m}$ due to the effect of the disturbance and noise.

4) *Frequency Domain Properties During Track-Following:* Now we shall examine the frequency domain properties of the servo system with the proposed control scheme during the track-following mode. The measured frequency response of the open-loop system with the proposed scheme is shown in Fig. 25, which clearly indicates that the proposed controller design achieves an acceptable level of closed-loop stability robustness, and 1.1 kHz servo bandwidth. In Fig. 26, we see the measured sensitivity and complementary sensitivity gain function of the closed-loop system, with the proposed control

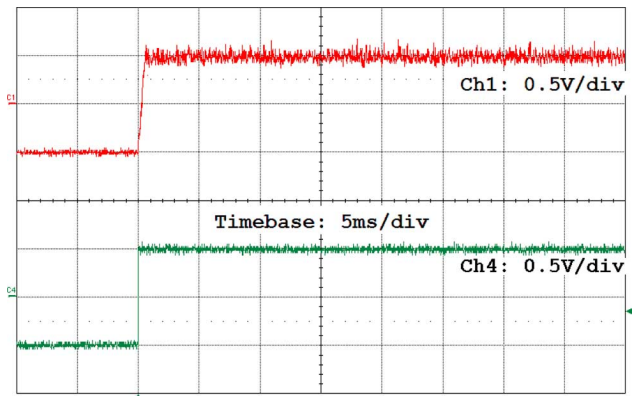


Fig. 23. UCS: Measured nominal $2 \mu\text{m}$ step response under the effect of disturbance and noise. Ch1: LDV-measurement ($2 \mu\text{m/V}$), Ch4: Trigger. Indicates the start of a nominal $2 \mu\text{m}$ seek.

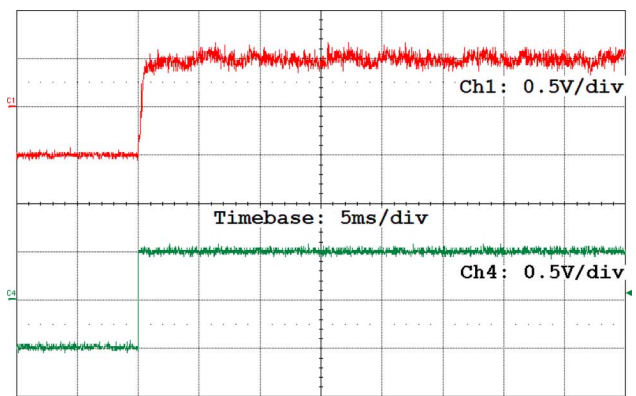


Fig. 24. CNF: Measured nominal $2 \mu\text{m}$ step response under the effect of disturbance and noise. Ch1: LDV-measurement ($2 \mu\text{m/V}$), Ch4: Trigger. Indicates the start of a nominal $2 \mu\text{m}$ seek.

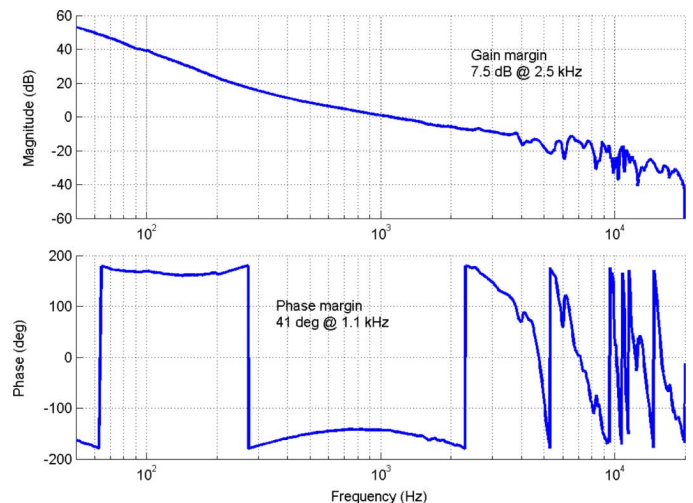


Fig. 25. Measured frequency response of open-loop function (LDV range $2 \mu\text{m/V}$).

scheme during track-following mode. The NRRO with the spectrum in Fig. 6 is added into the closed-loop during our experiment using dSpace. Consistently with the sensitivity and complementary sensitivity gain function in Fig. 26, the measured NRRO power spectrum as well as the cumulative

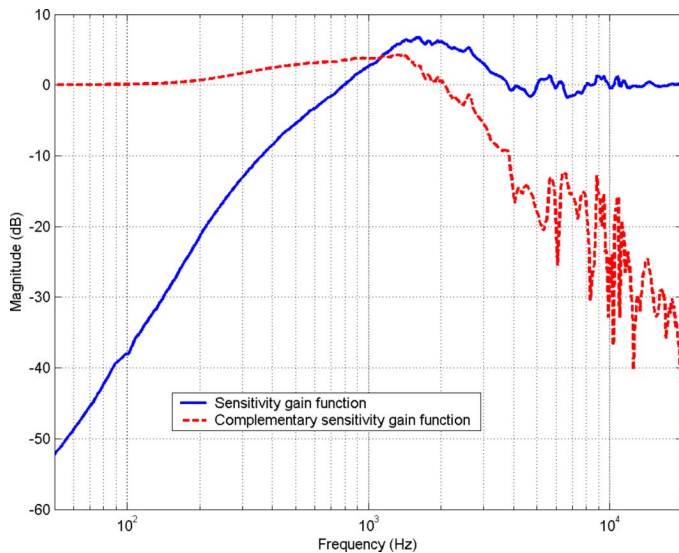


Fig. 26. Measured frequency gain response of sensitivity and complementary sensitivity function.

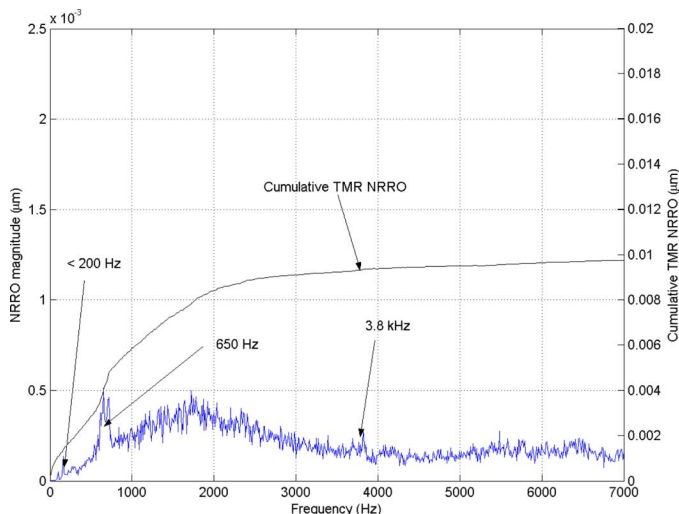


Fig. 27. Power spectrum of measured PES NRRO with servo control.

TMR NRRO are shown in Fig. 27. In terms of track-following accuracy, the proposed method reduces the 3σ (standard deviation) value of the true PES NRRO to 10.9 nm, which is 27.8% smaller than that prior to servo control.

Remark 5: Note that simulation and implementation results show this set of designed parameters work as well for 0.2 and 20 μm seek and the resulting control input is well within the saturation limit, which means fast and smooth track-seeking within 20 μm and high precision track-following can be achieved by using the same controller. However, with the conventional CNF scheme, controller must be retuned for any different seek length. Of course, for a larger seeking distance than 20 μm , the proposed controller needs to be redesigned to achieve excellent track-seeking performance.

VI. CONCLUSION

This paper has proposed a new nonlinear time-varying unified control scheme for track-seeking and track-following. By introducing two switching functions associated with general pa-

rameters and augmenting disturbance and noise models with the plant model, the proposed scheme is able to achieve fast and smooth seeking and also suitable for high accuracy track-following. Thus it has been proved to be more advantageous than the existing conventional scheme which involves a single nonlinear error function. The simulation and implementation results on a HDD application have verified the effectiveness of the proposed control scheme. It has been demonstrated that the proposed scheme can achieve a fast and smooth track-seeking and is completely insensitive to seek length variation within the range of 20 μm , and during track-following mode it has rejected more than 27% of the NRRO disturbance and noise.

ACKNOWLEDGMENT

The authors would like to thank K. Y. Lum and K. Peng of Temasek Laboratories, National University of Singapore, for their valuable suggestions.

REFERENCES

- [1] B. Hredzak, G. Hermann, and G. Guo, "A proximate-time-optimal-control design and its application to a hard disk drive dual-stage actuator system," *IEEE Trans. Magn.*, vol. 42, no. 6, pp. 1708–1715, Jun. 2006.
- [2] J. C. Doyle, B. A. Francis, and A. R. Tannenbaum, *Feedback Control Theory*. New Jersey: Macmillian Publishing Co., 1992.
- [3] B. M. Chen, T. H. Lee, K. Peng, and V. Venkataramanan, *Hard Disk Drive Servo Systems*, 2nd ed. New York: Springer, 2006.
- [4] A. A. Mamun, G. Guo, and C. Bi, *Hard Disk Drive: Mechatronics and Control*. Boca Raton, FL: CRC Press, 2006.
- [5] V. Venkataramanan, K. Peng, B. M. Chen, and T. H. Lee, "Discrete-time composite nonlinear feedback control with an application in design of a hard disk drive servo system," *IEEE Trans. Control Syst. Technol.*, vol. 11, no. 1, pp. 16–23, Jan. 2003.
- [6] B. M. Chen, T. H. Lee, K. Peng, and V. Venkataramanan, "Composite nonlinear feedback control for linear systems with input saturation: Theory and an application," *IEEE Trans. Autom. Control*, vol. 48, no. 3, pp. 427–439, Mar. 2003.
- [7] H. K. Khalil, *Nonlinear Systems*, 3rd ed. Englewood Cliffs, NJ: Prentice-Hall, 2000.
- [8] M. Hirata and M. Tomizuka, "Short track seeking of hard disk drives under multirate control-computationally efficient approach based on initial value compensation," *IEEE-ASME Trans. Mechatron.*, vol. 10, no. 5, pp. 535–545, Oct. 2005.
- [9] T. Yamaguchi, "Design points of mechatronics servo control – HDD servo control," presented at the IEEE Multi-Conf. on Syst. and Cont. Tutorial Workshop, Singapore, Sep. 2007.
- [10] G. Cheng, K. Peng, B. M. Chen, and T. H. Lee, "Improving transient performance in tracking general references using composite nonlinear feedback control and its application to high-speed XY-table positioning mechanism," *IEEE Trans. Ind. Electron.*, vol. 54, no. 2, pp. 1039–1051, Apr. 2007.
- [11] K. Peng, B. M. Chen, G. Cheng, and T. H. Lee, "Modeling and compensation of nonlinearities and friction in a micro hard disk drive servo system with nonlinear feedback control," *IEEE Trans. Control Syst. Technol.*, vol. 13, no. 5, pp. 708–721, Sep. 2005.
- [12] Y. Li, V. Venkataramanan, G. Guo, and Y. Wang, "Dynamic nonlinear control for fast seek-settling performance in hard disk drives," *IEEE Trans. Ind. Electron.*, vol. 54, no. 2, pp. 951–962, Apr. 2007.
- [13] G. F. Franklin, J. D. Powell, and A. Emami-Naeini, *Feedback Control of Dynamic Systems*, 4th ed. Englewood Cliffs, NJ: Prentice-Hall, 2002.
- [14] D. Abramovitch, F. Wang, and G. Franklin, "Disk drive pivot nonlinearity modeling Part I: Frequency domain," in *Proc. Amer. Control Conf.*, Baltimore, MD, Jun. 1994, pp. 2600–2603.
- [15] C. Du, L. Xie, G. Guo, J. Zhang, Q. Li, B. Hredzak, and J. N. Teoh, "A generalized KYP lemma based control design and application for 425 KTIPI servo track writing," in *Proc. Amer. Cont. Conf.*, 2006, pp. 1303–1308.

- [16] C. Du, J. Zhang, and G. Guo, "Vibration modeling and control design for self-servo track writing," Data Storage Inst., Singapore, Tech. Rep. ISSN 0218-4877, 2002.
- [17] H. S. Lee, "Controller optimization for minimum position error signals of hard disk drives," *IEEE Trans. Ind. Electron.*, vol. 48, no. 5, pp. 945-950, Oct. 2001.
- [18] J. K. Chang and H. T. Ho, "LQG/LTR frequency loop shaping to improve TMR budget," *IEEE Trans. Magn.*, vol. 35, no. 9, pp. 2280-2282, Sep. 1999.
- [19] G. Cheng, B. M. Chen, K. Peng, and T. H. Lee, "A MATLAB toolkit for composite nonlinear feedback control," in *Proc. 8th Int. Conf. Control, Auto., Robot., Vis.*, Dec. 2004, pp. 878-883.
- [20] K. S. Narendra and A. M. Annaswamy, *Stable Adaptive Systems*. Mineola, NY: Dover, 2005.



Chin Kwan Thum (S'07) received the B.Eng. (honors) degree in electrical and computer engineering from National University of Singapore (NUS), Singapore, in 2004, where he is currently pursuing the Ph.D. degree in electrical engineering.

His current research interests include the areas of linear and nonlinear control theories and applications in designing robust high performance servo controller for future ultrahigh density storage systems.



Chunling Du (M'00-SM'07) received the B.Eng. and M.Eng. degrees in electrical engineering and the Ph.D. degree in electrical engineering from Nanjing University of Science and Technology, Nanjing, China, in 1992, 1995, and 2000, respectively.

She joined A*STAR Data Storage Institute (DSI), Singapore, in 1999, as a Research Engineer. She is currently a Senior Research Fellow in the Mechatronics and Recording Channel Division, DSI. She is also an Adjunct Assistant Professor with NTU.

Her research interests include optimal and robust control, vibration modeling and control, advanced control and mechatronics for nanopositioning systems, signal processing, and multidimensional systems. She has published a few papers and coauthored (with L. Xie) the monograph *H_∞ Control and Filtering of Two-Dimensional Systems* (Springer, 2002).



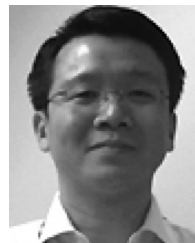
Ben M. Chen (S'89-M'91-SM'00-F'07) received the B.S. degree in mathematics and computer science from Xiamen University, China, in 1983, the M.S. degree in electrical engineering from Gonzaga University, Spokane, WA, in 1988, and the Ph.D. degree in electrical and computer engineering from Washington State University, Pullman, WA, in 1991.

He was a Software Engineer with South-China Computer Corporation, Guangzhou, China, from 1983 to 1986, and was an Assistant Professor from 1992 to 1993 with the Department of Electrical

Engineering, State University of New York at Stony Brook. Since August 1993, he has been with Department of Electrical and Computer Engineering, National University of Singapore, where he is currently a full Professor. His current research interests are in robust control, systems theory, control applications, the development of unmanned helicopter systems and financial market modeling.

He is the author/coauthor of seven research monographs including *Linear Systems Theory* (Birkhäuser, 2004), *Robust and H_∞ Control* (Springer, 2000) and *Hard Disk Drive Servo Systems* (Springer, 1st Ed., 2002; 2nd Ed., 2006).

Dr. Chen was a recipient of the Best Poster Paper Award at 2nd Asian Control Conference, Seoul, Korea (1997); University Researcher Award, National University of Singapore (2000); Prestigious Engineering Achievement Award, Institution of Engineers, Singapore (2001); Temasek Young Investigator Award, Defence Science and Technology Agency, Singapore (2003); Best Industrial Control Application Prize at 5th Asian Control Conference, Melbourne, Australia (2004); and elected to IEEE Fellow. He is an Associate Editor with many international journals including IEEE TRANSACTIONS ON AUTOMATIC CONTROL, *Automatica*, and the *Systems and Control Letters*.



Eng Hong Ong received the B.Eng. (honors) and Ph.D. degrees in mechanical engineering from National University of Singapore (NUS), Singapore.

Presently, he is the Manager of the Mechatronics and Recording Channel Division of A*STAR Data Storage Institute (DSI), Singapore. He is also an Adjunct Assistant Professor with the Mechanical Engineering Department, NUS. His research interests include finite-element method, multibody dynamics, and mechatronics. He works closely with both academia and industry to develop next

generation HDDs.



Kim Piew Tan received the B.Eng. (honors) and Ph.D. degrees in mechanical engineering from University of Sheffield, South Yorkshire, U.K., in 1997 and 2002, respectively.

He joined A*STAR Data Storage Institute (DSI), Singapore, in 2004, as a Senior Research Fellow. His current research interests include dynamics and vibration analysis, and control applications for mechanical and data storage systems.